ELSEVIER

Intermetallics 7 (1999) 1059–1068

Intermetallics

Pinning of dislocations and the origin of the stress anomaly in FeAl alloys

D.G. Morris*, C.T. Liu , E.P. George

Metals and Ceramics Division, Oak Ridge National Laboratory, Oak Ridge, TN 37831-6115, USA

Received 15 February 1999; accepted 23 February 1999

Abstract

The anomalous stress rise found at intermediate temperatures in FeAl alloys may be caused by the presence of thermal vacancies produced as the temperature rises. Strong support for this hypothesis is provided by the demonstration that the same absolute values of stresses as well as stress increases are found both when testing at high temperatures and when testing at room temperature samples quenched from the same high temperatures. Examination of the superdislocations present after deformation shows strong pinning only at jogs produced by intersection with forest dislocations. Such sessile jogs on screw superdislocations lead to dipole and loop formation as the dislocations continue moving, hence producing the debris observed after deformation. In addition, edge superdislocations show a stepped morphology caused by line instabilities over a certain range of directions. There is no evidence of strong pinning and associated dislocation bowing by vacancy-aggregate type obstacles, and it is, therefore, deduced that the pinning obstacles responsible for the anomalous stress increase are probably relatively weak single vacancies, rather like solute atoms, and not stronger multi-vacancy defects. © 1999 Elsevier Science Ltd. All rights reserved.

Keywords: A. Iron aluminides (based on FeAl); B. Mechanical properties at high temperatures; B. Mechanical properties at ambient temperature; D. Defects: point defects; D. Defects: dislocation geometry and arrangement

1. Introduction

There has been much debate recently about the origin of the stress anomaly in FeAl alloys [1,2]. Several mechanisms of dislocation pinning have been proposed to explain the increase of flow stress over the temperature range of about 300–550°C, where APB-dissociated <111> superdislocations control deformation: mechanisms such as pinning by cross-slip of one or both of the 1/2<111> partial dislocations [3], decomposition into poorly mobile <100> or <110> dislocations [4–6], and climb of the partials have been proposed [7]. At high temperatures the flow stress falls as such pinning obstacles are overcome, possibly as the change from a <111> to a <100> dislocation Burgers vector takes place [5,6,8], or alternatively as climb processes allow the easy movment of the <111> superdislocations [9–11]. Recently, an alternative mechanism for the hardening anomaly has been proposed [11,12] based on the influence of a solution of thermally-produced vacancies. This theory developed from the experimental observation of strong hardening [13,14] due to the high vacancy concentration [2,13,15,16] retained in samples quenched from high temperatures.

Several experiments reported recently support the model of vacancy hardening as responsible for the anomalous hardening. Two important examples are given here: (a) the observation of a prior-soaking-time dependence of the anomalous stress increase, that is, that some time is required at the high temperature for the hardening to arise [17,18]; (b) the observation that very similar hardening is achieved on testing at a temperature in the range of anomalous strengthening, or on testing at room-temperature, material which has been quenched from the same high temperature [19,20]. Both observations strongly support the vacancy-hardening model, whereby hardening requires the creation of the equilibrium population of vacancies, which takes some time at high temperature and is, thereafter, a characteristic of the crystal at temperature or when quenched. Mechanical behaviour is clearly determined by the dislocation-point defect interactions, and does not rely on

* Corresponding author now at Department of Physical Metallurgy, CENIM, CSIC, Avenida Gregorio del Amo 8, 28040 Madrid, Spain.

0966-9795/99/$ - see front matter © 1999 Elsevier Science Ltd. All rights reserved.
PII: S0966-9795(99)00015-1

the dislocations carrying out some thermally-activated process (cross-slip, climb, etc.). The second observation reported here, of similar flow stress increases when testing quenched material at room temperature, or on testing at the same high temperatures (over the range of the anomalous stress rise) has not been strongly emphasized before, and is demonstrated in Fig. 1 for polycrystalline FeAl with near 40% Al. Accepting some scatter of data due to differences of impurity content or grain size, it is clear that the high-temperature data (until the anomalous stress peak is reached) and the room-temperature data on quenched material are almost identical and show the same general temperature dependence.

While the general idea seems clear that point defects created at high temperature are responsible for hardening, envisaged as a form of solute-hardening, there are several aspects of the hardening phenomenon that remain unclear. The extent of hardening is very strong, as characterised by a hardening coefficient (strength increase divided by the square root of the vacancy concentration) of the order of $G/30$ (G is the shear modulus), in comparison with a hardening coefficient of the order of $G/760$ for antisite defects or for typical solute additions [2,14]. This has led several workers to surmise that the important point defects may be present not in the form of invidual vacancies but as vacancy aggregates [2,21,22] Another aspect of mechanical behaviour that remains as yet unexplained by the vacancy-solute hardening model is the significant dependence of the anomalous hardening on crystal orientation [5].

The present study set out to examine the room-temperature dependence of strength of a FeAl alloy with 40 at% Al after quenching from different temperatures over the range of the anomalous stress peak found on high-temperature testing, and to examine the dislocation structures created on deforming such materials,

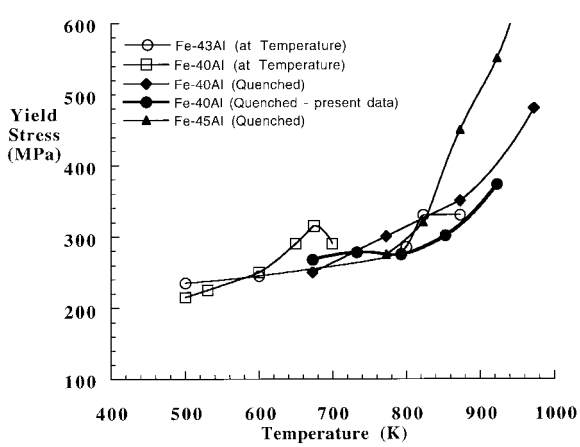

Fig. 1. The variation of high-temperature flow stress and room-temperature flow stress on quenched material. Polycrystalline FeAl samples with Al content near 40%. Literature data taken from Refs. [8,11,18–20].

looking especially for indications of dislocation pinning or evidence of dislocation-point defect interactions.

2. Analysis of dislocation-obstacle interactions due to vacancy hardening

The extent of hardening achieved by quenched-in vacancies has been examined [11,14] in terms of the Fleischer model of solute hardening [23], whereby a randomly distributed population of stationary vacancies interacts with dislocations when the dislocation cores are in the very close vicinity of the vacancies. Such a model predicts hardening that is proportional to the square root of the vacancy concentration ($\sqrt{c}$). The exact nature of the vacancy-dislocation interaction is not defined, and in the classical theory is caused by elastic misfit or modulus differences between the solute atom (vacancy) and the matrix atom. While the vacancy sits on the dislocation core it can also be imagined to create a close jog pair, but there will not be trailing antiphase boundary (APB) faults as the dislocation moves away and detaches itself from a stationary vacancy. Foreman and Makin [24] have also examined the behaviour of dislocations passing through a population of obstacles (solute or particles) in terms of the intensity of the elementary obstacle-dislocation interaction, and described the strengthening obtained in terms of the bowing angle (ϕ) of the dislocation as it breaks through the obstacle. For the case where the strength of the elementary interaction is relatively weak and the breakaway angle large, the strengthening can be written as $m\mu b\{\cos(\phi/2)\}^{3/2}/\lambda$, where m is the Taylor factor for the material (taken as about 2.5 for the bcc based material), μ is the shear modulus ($\approx$50 GPa), b the Burgers vector ($\approx$0·25 nm for the $1/2<111>$ dislocation), and λ the average separation of the solute atoms (vacancies) in the glide plane, with $\lambda = N^{-1/2}$, and N the number of obstacles per unit area. As shown by Fleischer [23], the value of λ can be written as $2a/\sqrt{c}$, where a is the atomic size and c the concentration of solute (vacancies). For a relatively weakly interacting solute, as expected for vacancies, the mean distance between obstacles on a dislocation line is somewhat increased [24] as the dislocation bows between the obstacles, and the mean segment length λ_F becomes $\lambda/\sqrt{\{\cos(\phi/2)\}}$.

These ideas can be applied to the present case, where a population of vacancies is believed to produce the observed strengthening, to deduce expected values for obstacle spacings and dislocation bowing angles at breakaway. Based on strengthening of about 100 MPa at a temperature of about 600°C (see Fig. 1), and assuming vacancy formation enthalpies and entropies [2,15,16] of $\Delta H_v \approx 91$ kJ/mol and $\Delta S_v \approx 4.6\ K$ (where K is the Boltzmann constant), likely values for vacancy concentration, dislocation segment lengths and breakaway

Table 1
Point defect density, c, spacing between point defects, λ, bowing angle, ϕ, of a dislocation segment as it breaks through an obstacle, and average segment length at breakthrough λ_F (see text for details)[a]

Point defect type	Point defect concentration c	Average defect spacing λ	Critical bowing angle ϕ	Segment length λ_F
Mono-vacancy	4×10^{-4}	25 nm	160°	58 nm
Di-vacancy	7×10^{-5}	76 nm	134°	122 nm
Tri-vacancy	1×10^{-5}	199 nm	84°	231 nm

[a] Data correspond to Fe–40Al at about 600°C where strengthening of 100 MPa is achieved.

angle are shown in Table 1. It may be seen that the many vacancies present are confirmed to be relatively weakly interacting species, but nevertheless the combined effect of these many weak obstacles can be the strengthening observed. An alternative possibility, suggested by various authors [2,21,22], is that the important interacting species may be vacancy aggregates such as divacancies, trivacancies, etc. Corresponding concentrations and dislocation interactions leading to the same observed strengthening are also shown in Table 1, where the following suppositions have been made for enthalpies and entropies of aggregate formation: $\Delta H_{2v}\approx1.5\ \Delta H_v$ or 136.5 kJ/mol, and $\Delta S_{2v}\approx1.5\ \Delta S_v$ (based on assessments by Yoshimi et al. [21]), and $\Delta H_{3v}\approx2\ \Delta H_v$ and $\Delta S_{3v}\approx 2\ \Delta S_v$. The data relating to divacancies and trivacancies are no more than crude estimates and extrapolations, and serve no further than to indicate the elementary aggregate-dislocation interaction necessary to explain the observed strengthening as the obstacle density changes.

It is clear from this analysis that the observed strengthening may be produced by a large number of close obstacles, each weakly interacting with the dislocation line, or by a smaller number of more widely spaced, strongly-interacting obstacles. This analysis also emphasizes that a given density of obstacles, with a given intensity of dislocation-obstacle interaction, will produce material hardening irrespective of the physical nature of the obstacle itself, that is, whether it is a vacancy-type point defect, or a small cross-slipped, climbed, or decomposed dislocation segment. For each type of pinning object, however, we can make certain suppositions about the obstacle and its characteristics, for example: whether there will be interaction with screw or edge dislocations; whether the dislocation will retain its <111> Burgers vector at the obstacle or be changed (as by decomposition); whether one or both partials of the superdislocation will be affected; what the length dimension of the obstacles is? These various characteristics are summarised in Table 2 for the various possible pinning obstacles, and will be the features examined in detail in the present study.

3. Experimental details

The present experiments were carried out on a Fe-40 at% Al alloy prepared by arc-melting and drop-casting, homogenisation, extrusion, and recrystallization to a uniform grain size of about 300 μm by an anneal for 2 h at 1000°C and air cool. All samples were then annealed for 7 days at 400°C followed by an oil quench to ensure a low vacancy concentration and removal of much of the dislocation debris resulting from vacancy annihilation. Different samples were then annealed separately for long times (typically 5–7 days) at temperatures of 460, 520, 580 and 650°C, followed by an oil quench, to retain the equilibrium vacancy population corresponding to each temperature. It should be noted that the highest annealing temperature is above that of the stress peak found during high-temperature testing, but would be expected to show considerably more hardening than the other samples because of its higher vacancy content. Samples for compression were machined from the annealed blocks, and compressed in air at room temperature at a strain rate of about 1×10^{-3}/s to a strain of about 1–1.5%. Typically, three samples were tested for each annealing condition. Some of the samples showed

Table 2
Characteristics of the expected interaction of a <111> superdislocation with possible pinning obstacles in FeAl alloys

Obstacle/characteristic	Vacancy (aggregate) obstacle	Small cross-slipped segment	Small decomposed segment
Interaction with edge or screw dislocations	Edge	Screw	Edge
Burgers vector at obstacle	<111>	<111>	<100> and <110>
One or two partials of superdislocation	One	One	Two
Length of obstacle	$\approx b$ (Burgers vector)	$\approx d$ (superpartial separation)	$\approx d$(superpartial separation)
Schematic illustration			

slight serrations on the load-extension plots, similar to those noted by Yoshimi et al. [21], but these were not systematically found and were not more obvious for samples quenched from either high or low temperatures. In addition hardness testing was carried out to monitor changes of mechanical strength.

Samples for TEM were prepared by twin-jet electropolishing on disks cut at 45° to the loading axis, and were examined in bright-field and weak-beam conditions using Philips CM12 and CM30 instruments. Most of the weak-beam analyses were carried out on the CM12 instrument to avoid possible irradiation damage interactions with dislocations and quenched-in defects. Dislocation Burgers vector analysis, and determination of dislocation line directions and glide planes, were performed using standard image contrast and stereographic techniques.

4. Results

Flow stresses (at 0.2% plastic strain) determined at room temperature on quenched material are shown in Fig. 1 in comparison with literature data [8,11,18–20] on FeAl alloys of similar composition tested either after the same quenching procedure or at high temperature. All the results show very similar temperature dependencies, with perhaps the exception of the Fe-45Al material [19] which shows a steeper increase in stress with temperature (as expected for its high Al content), and one Fe-40Al material [8,11] which shows a faster stress rise to an stress peak at a notably lower temperature. Hardness measurements on the present samples showed an increase with quenching temperature very similar to the flow stress increase measured during compression testing, Fig. 2. The hardness values (when expressed in MPa) are about ten times the yield stress values instead of the three times expected, for reasons that are not understood, but which may be related to the high work-hardening associated with ordered materials. The slower increase in hardness than in yield stress on quenching from higher temperatures would then correspond to the larger effect of quench state on yield stress than on work-hardening, as demonstrated by Yang and Baker [20].

Fig. 3 shows the general microstructure observed after straining a quenched material at room temperature. The dislocation microstructure is characterised by fairly long dislocation segments, with both long edge segments and long screw segments observed, as well as a high density of fine dipoles and small loops. These are $<111>$ superdislocations lying on {110} planes. Many of the dislocations are slightly bowed, and we can argue that these have essentially retained their position during unloading on the grounds that the extent of additional hardening due to the presence of fine obstacles produced by the prior high temperature treatment is smaller than the strength of frictional forces due to Peierls lattice effects. The extent of bowing observed is consistent with this. Occasionally $<100>$ dislocations are observed, often as widely spaced straight and nearly parallel pairs of dislocations, which often react with the $<111>$ glide dislocations, and are believed to be the remnants of the dislocation structures produced during annealing and vacancy annihilation [25]. The microstructure appears to

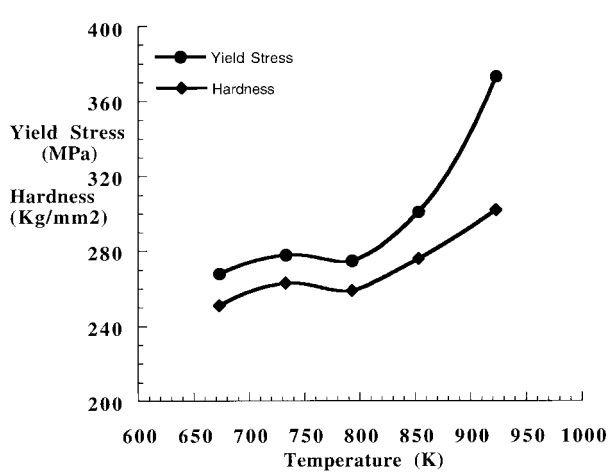

Fig. 2. Variation of yield stress and hardness measured in quenched Fe–40Al as a function of the temperature prior to quenching.

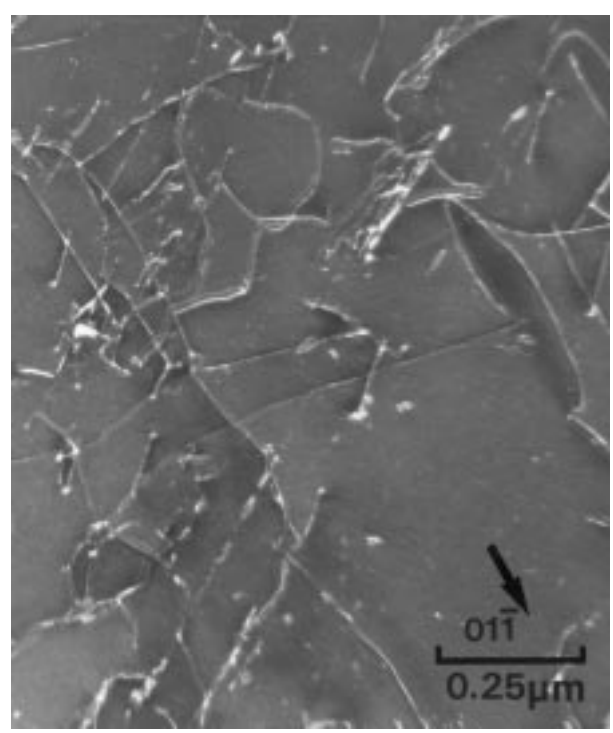

Fig. 3. Weak beam micrograph showing typical dislocation structures in a sample deformed at room-temperature after a quench from 580°C. Zone axis (ZA) is near [011] and **g** vector is 01$\bar{1}$, imaging conditions about **g**: 5–6 **g**.

be similar for all the material conditions examined, irrespective of the temperature prior to quenching.

When examined at high magnifications, many of the edge dislocations show serrations along their length, Fig. 4. Such effects were seen for all tested samples, irrespective of the quench temperature, and correspond closely to the elastic instabilities noted by Crawford et al. [26,27]. In the present study, such dislocation-line instabilities were not found for near-screw dislocations, but for edge dislocations over the line direction range about 90–150°, similar to the earlier studies [26,27]. The observation of such effects for the softer materials quenched from low temperatures as well as for the harder materials after high-temperature quenches shows that such instabilities play no significant role in controlling dislocation behaviour and flow stresses.

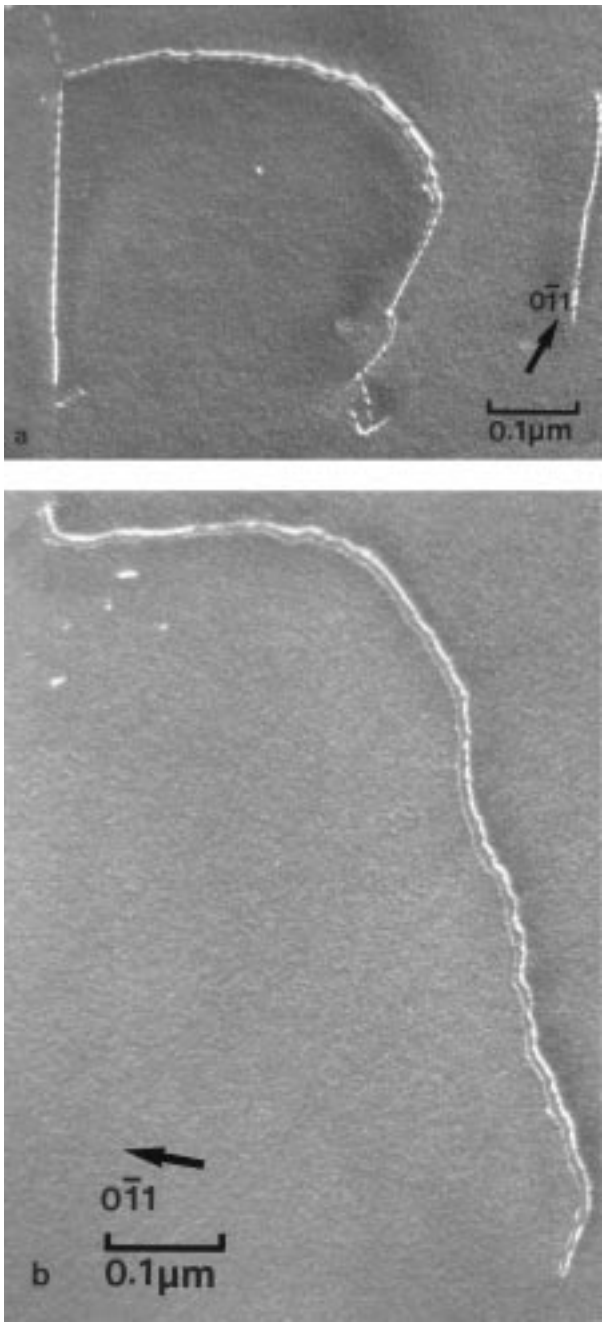

Fig. 4. Weak beam micrographs showing instabilities of line directions for near-edge superdislocations in samples quenched from (a) 400°C and (b) 650°C. ZA near [011] and **g** vector 0$\bar{1}$1 for both with imaging conditions near **g**: 5–6 **g**.

On some occasions, similar edge dislocations appear to show cusps along their lengths, see Fig. 5, where the superpartial dislocations may come closer together as though retained by some undetected obstacle. Between the pinning points the short dislocation segments are slightly bowed, corresponding well to the effective stress operating during deformation. Such features will be examined in more detail below. Again, importantly, the frequency of such pinning obstacles hardly changes with quenching temperature, with bowed dislocation segment lengths being typically about 50–100 nm for all quench temperatures.

Screw dislocations show strong pinning points occasionally along their lengths, where dipoles or eventually disconnected loops form during continued deformation, Fig. 6. Such effects are probably produced after the intersection of the moving superdislocations with forest dislocations, and presumably are the origin of the dipole and small loop debris shown earlier (Fig. 3). The distance between such jogs on the screw dislocations is of the order of 300–500 nm. Fig. 6a shows a screw dislocation forming several dipoles along its length, and then rotating to become an edge dislocation with fine serrations due to the elastic instability. This edge dislocation has encountered a $<100>$ dipole, presumably grown-in during the prior vacancy annihilation procedure, which does not appear to have any other effect than a local change of dislocation direction due to elastic field interactions. These observations could be made in all the samples examined, irrespective of the temperature prior to the quench.

The fine pinning points found on edge dislocations are examined in detail in Fig. 7. Imaging using several diffraction conditions confirms that the pinning points act on both partials of the $<111>$ superdislocation, that the Burgers vector remains the same along the dislocation as it reaches the obstacle, such that there is no recombination or decomposition of dislocations at the obstacle, while tilting the dislocation about its length direction shows that the dislocation and its drawn-out pinning "teeth" lie on same glide plane. These pinning points are not consistent with any of the pinning mechanisms illustrated in Table 2, and are most likely produced by the intersection of the gliding edge dislocation with forest dislocations, leading to a pair of jogs on the glissile dislocation and the formation of dragging APB tube debris. Since such features were observed in similar numbers in all material conditions,

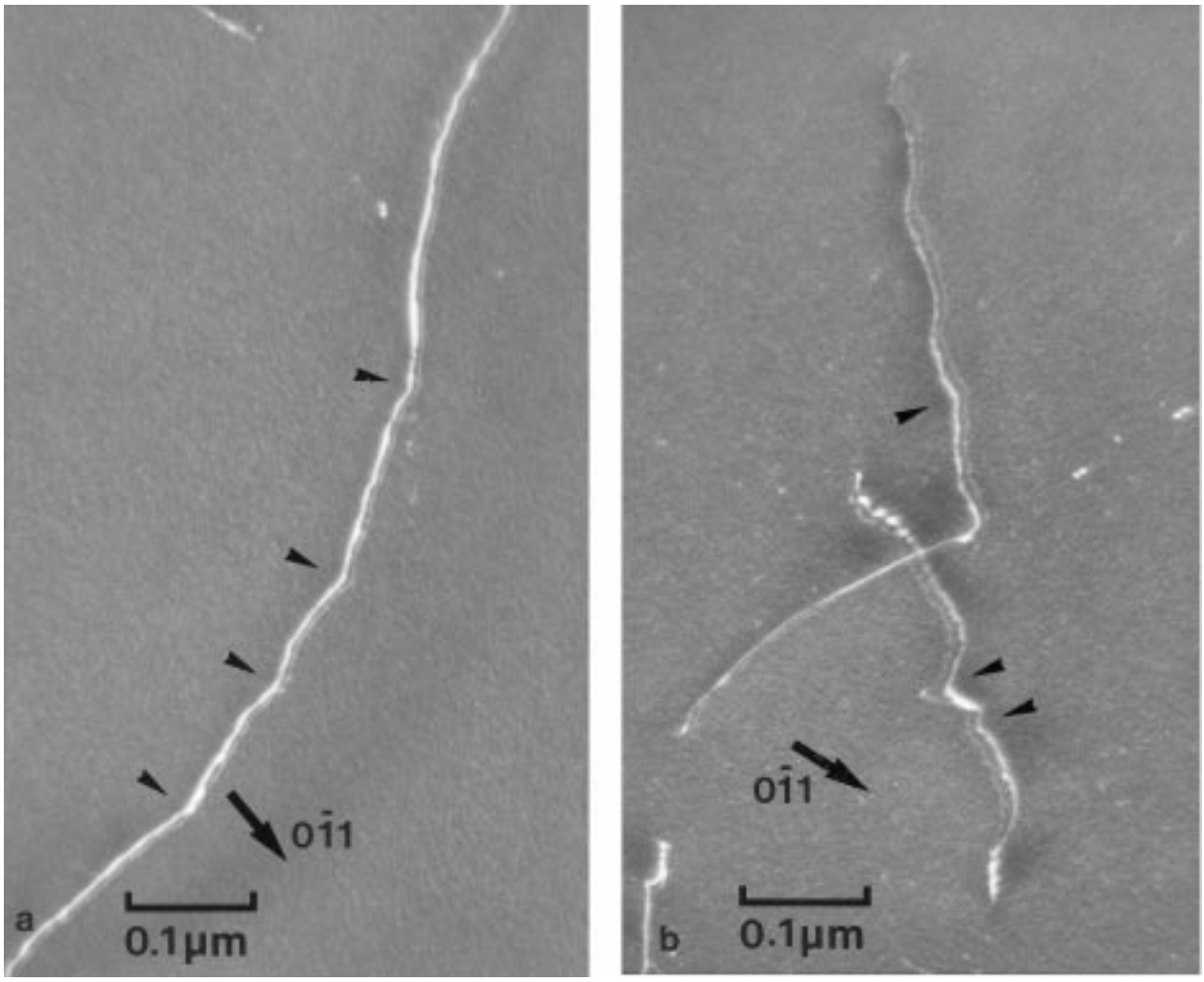

Fig. 5. Weak beam micrographs showing fine cusps, some arrowed, separating gently bowed segments on edge superdislocations in samples quenched from (a) 400°C and (b) 650°C. ZA near [011] and **g** vector 0$\bar{1}$1 for both with imaging conditions about **g**: 5–6 **g**.

irrespective of quench temperature, the density of quenched-in vacancies or aggregates should play no role in their formation.

Fig. 8a shows a superdislocation with a discontinuity along its length similar to that near the "teeth" in Fig. 7. This discontinuity has been shown to be due to a short forest dislocation attached to the long dislocation, so producing a pair of jogs. When such jogs are not aligned along the direction of dislocation motion they will trail an APB tube, and some indication of such APB trails is shown in Fig. 8b, the long features in weak contrast.

5. Discussion

One of the most important observations emphasized in the present study (see Fig. 1) is the strong similarity of strength variation on testing Fe–Al samples with near 40% Al at high temperatures, where the anomalous stress increase is observed, and on testing at room temperatures samples which have been quenched from the same high temperatures. This observation confirms that such strengthening is a matrix property, as produced by the point defect populations, and not a property of dislocation locking by some thermally activated process. It also provides support of the claim that the point defects present at high temperatures have been reasonably retained by the quench procedure used.

During deformation, dislocations bow and break past obstacles under the action of the effective stress, which is smaller than the applied stress due to the action of friction stresses, for example Peierls stresses. Many of the dislocations observed in the present study are seen to be slightly bowed, and estimates of the effective stress based on such curvature give values of the order of 50-100 MPa. This may be considered a reasonable estimate of the true effective stress during deformation and confirms that the dislocations have not moved extensively during unloading, but have essentially retained their configurations occupied during testing.

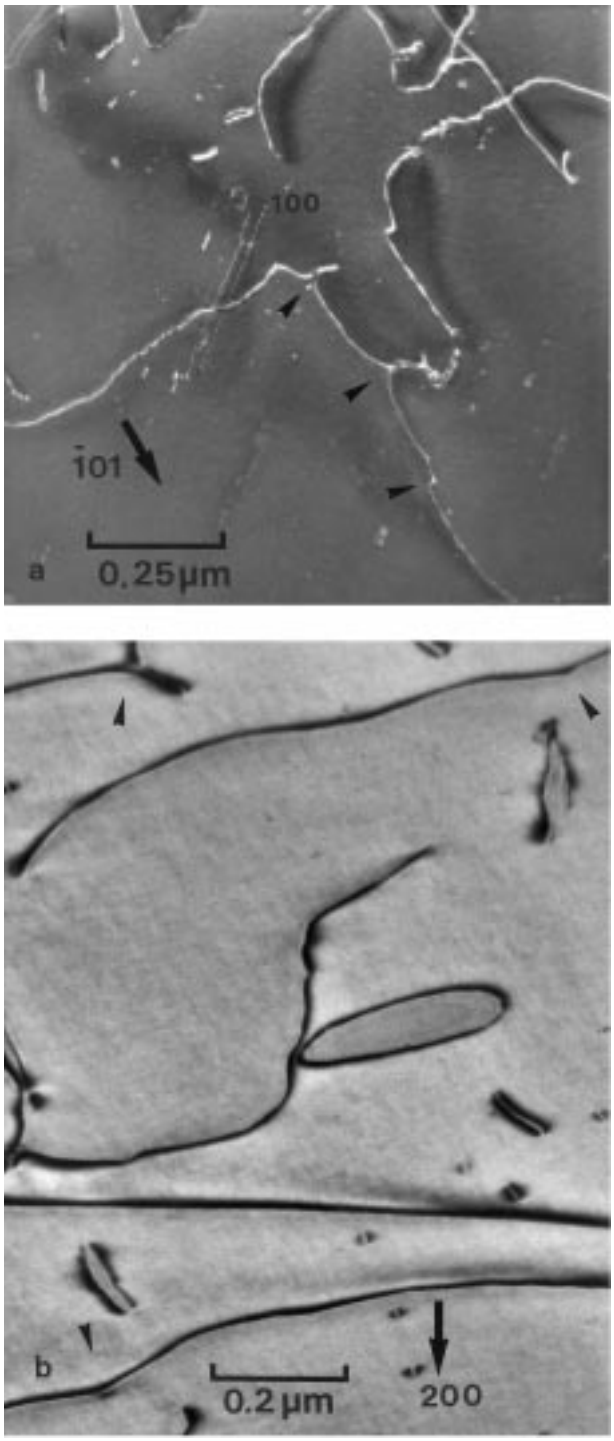

Fig. 6. Weak beam micrographs showing fine cusps and dipoles, some arrowed, separating gently bowed segments on screw superdislocations in samples quenched from (a) 580°C and (b) 650°C. ZA: (a) near [111] and **g** vector $\bar{1}01$; (b) near [011] and 200; in both cases imaging conditions are near **g**: 5–6 **g**. In (a) a screw dislocation rotates to an edge direction and then shows elastic line instability. The edge dislocation passes near a straight 100 dipole.

An analysis based on the Fleischer/Foreman-Makin models has estimated the strengthening due to a given population of point defects in terms of the intrinsic strength of each individual obstacle (and the dislocation bowing angle ϕ as the dislocation breaks through). For a given density of vacancies or aggregates, deduced from experimental or estimated values for vacancy/aggregate formation enthalpies and entropies, the observed magnitudes of strengthening may then be explained in terms of the characteristic intrinsic strengths of the obstacles and their corresponding bowing angles. Single vacancies are clearly relatively weak obstacles, producing only slight dislocation bowing, while multiple-vacancy aggregates are stronger obstacles and are associated with larger extents of dislocation bowing. This analysis has provided the basis of the present dislocation examinations, in an attempt to deduce the important type of pinning obstacle from the extent of dislocation bowing at the obstacles present.

The present study has shown several forms of dislocation pinning of the $<111>$ superdislocations responsible for deformation. Screw dislocations show strong pinning, with dipoles being dragged out leading eventually to the formation of dislocation loops of a variety of sizes (see Fig. 6 for dipoles forming on screw dislocations, and Fig. 3 for the variety of dislocation loops formed by deformation). Edge dislocations show two particular features, namely the onset of a stepped morphology for some line directions due to line tension instabilities (see Fig. 4), and a gently-bowed, short segment appearance (for example Fig. 5). The stepped morphology due to line instability has been analysed before (26,27), and is found in the same way for samples heat-treated at high and at low temperatures, with its appearance apparently depending only on the line direction. It is not believed to play any role in the anomalous strengthening. The cusps defining the gently-bowed segments have been shown to be present on both partials of the superdislocations with no change of either Burgers vector or habit plane (see Fig. 7). The most likely explanation for such cusps is the intersection of the mobile superdislocations and forest dislocations, leading to the formation of a pair of jogs. Some support for this is given by the observed density of such jogs, as well as the appearance of APB trails left behind after deformation (see Fig. 8), while the possibilities of material strengthening being due to cross slip or decomposition locking are eliminated. The density of such cusps (jogs) appeared similar for all samples examined, independent of the prior quenching temperature, confirming that quenched-in vacancies or aggregates were not the origin of such features. The density of such jogs is also consistent with the amount of strain imposed (1%) and the observed dislocation density ($\approx 10^{13}/m^2$ in Fig. 3 or 6): assuming the forest dislocation density is about half the total density, and a mean dislocation displacement of about 1–2 μm occurs during straining, jogs can be expected to be separated by distances of the order of 100 nm. The jogs observed on edge dislocations are separated

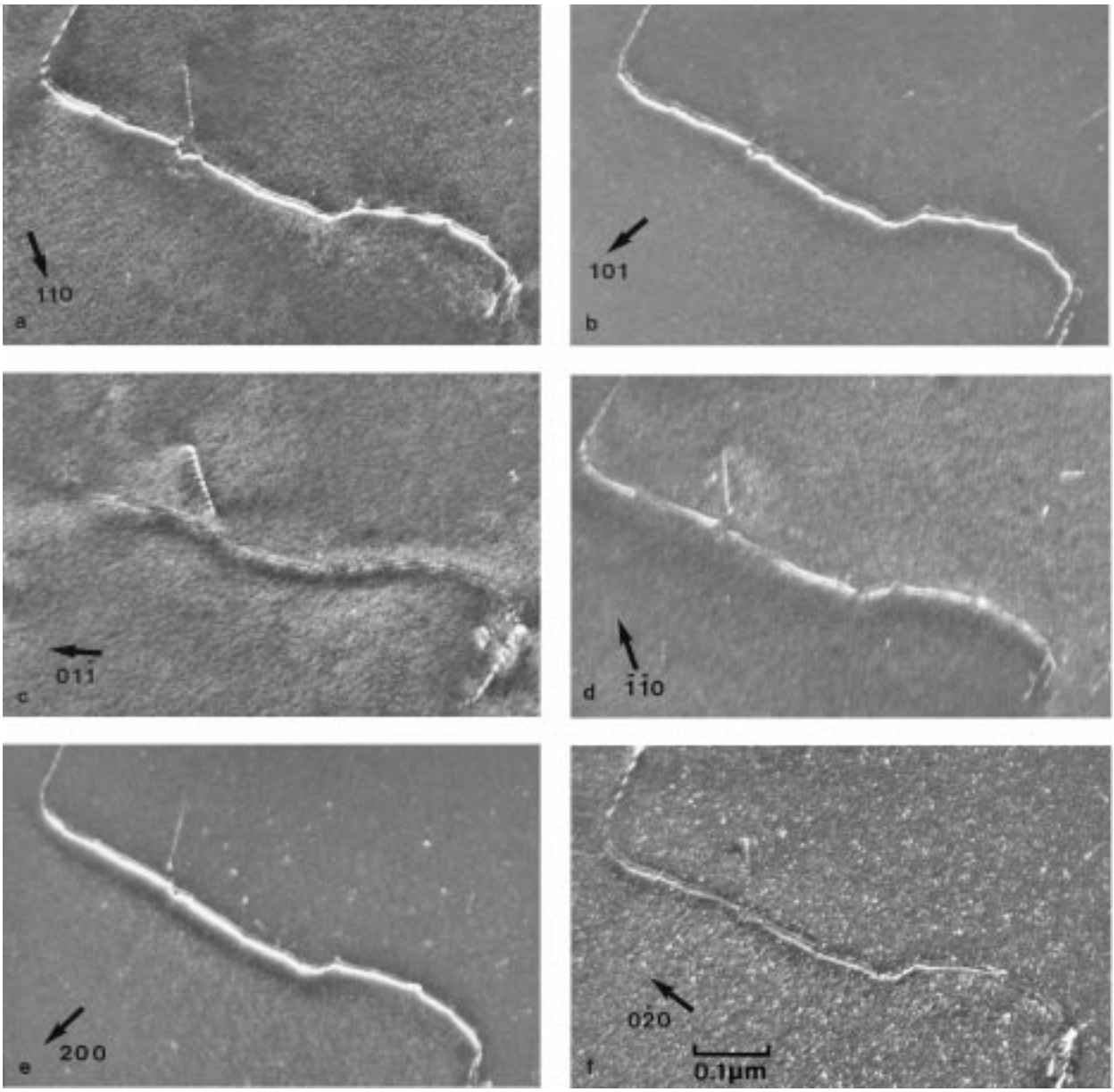

Fig. 7. Analysis of pinning points on an edge <111> superdislocation in a deformed sample quenched from 580°C. A weak beam condition of **g**: 3–6 **g** was used, depending on the particular case. (a) ZA near $[1\bar{1}2]$, **g** vector 110; (b) ZA near $[1\bar{1}1]$, **g** vector 101; (c) ZA near $[1\bar{1}1]$, **g** vector $01\bar{1}$; (d) ZA near $[1\bar{1}2]$, **g** vector $\bar{1}\bar{1}0$; (e) ZA near [001], **g** vector 200; (f) ZA near $[\bar{1}01]$, **g** vector $0\bar{2}0$.

by distances of the order of 50–100 nm (Fig. 5), while the jogs observed on screw dislocations are separated by distances of the order of 300–500 nm (Fig. 6), which is consistent with the higher mobility expected from edge superdislocations in these intermetallics at room temperature.

The dislocation structures observed are in most senses similar to those seen after deformation at temperatures near but below the stress anomaly peak, but there are some subtle differences. The fine details of serrations seen on edge dislocations, due to line instabilities, are not seen at high temperatures. This may be because such instabilities do not occur at high temperatures, due to changes of elastic parameters, or, more likely, that higher dislocation mobility and lower Peierls friction at the high temperatures allow the dislocation line to be smoothed and to remain smooth. Cusps due to jogs are also uncommon after high temperature deformation, possibly because the jogs may move along the dislocation lines to be annihilated. In both cases, the absence of elastic instabilities and intersection jogs after high temperature deformation confirms that these are low temperature features which do not play a role in producing the stress anomaly. Only a few <100> dislocations are seen after deforming the quenched samples here, and these were clearly present in the quenched state. There was no

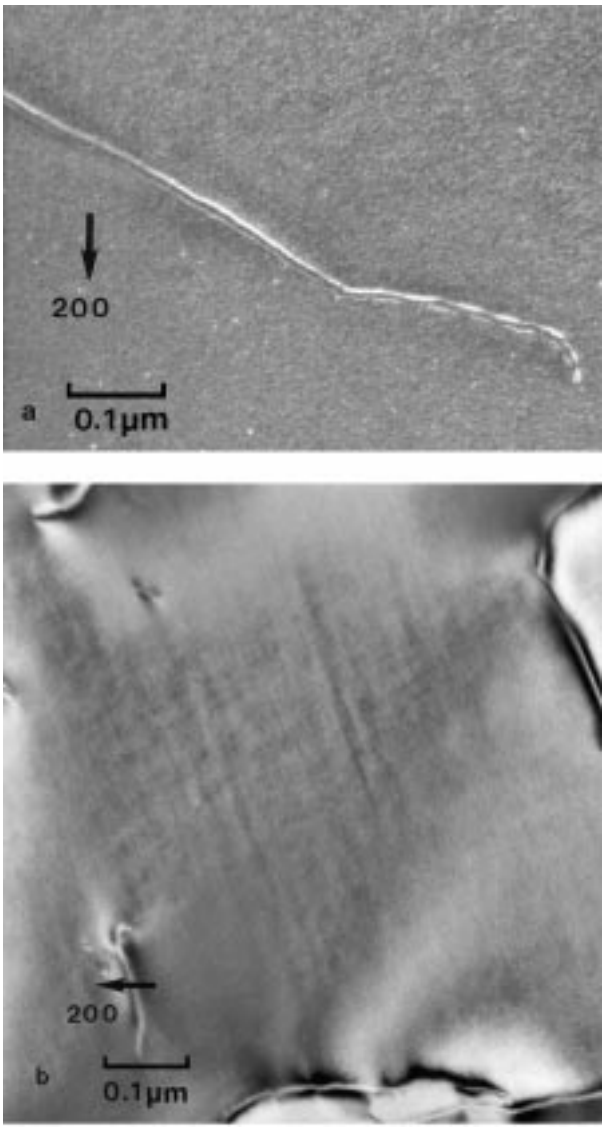

Fig. 8. (a) Superdislocation in a deformed sample quenched from 400°C showing the formation of a pair of jogs where a short segment of forest dislocation intersects. ZA near [011], **g** vector 200, weak Beam micrograph, imaging condition near **g**: 5–6 **g**. (b) Weak trails due to APB formation by dragging jogs on glissile superdislocations. ZA near [011], **g** vector 020, bright field image.

evidence that the formation of <100> segments from superdislocations plays any role in determining the stress increase. Equally, of course, no climb-locking could take place during the present room-temperature deformation, and there was no evidence of such climbing occurring.

There is little visual evidence here of any significant pinning of the superdislocations by any obstacle other than the intersections jogs (and perhaps some influence of the line instability effect). No bowing of the dislocations over notable bowing angles has been observed, apart perhaps from some very minor dislocation pinning (see Fig. 5) between the major cusps. Such minor pinning may, at least in some cases, be due to the line instability effect. The absence of any sign of significant pinning, apart from that due to the intersection jogs, is taken to mean that the vacancies are present as relatively weak obstacles and hence, based on the approximate calculations summarised in Table 1, that they should be present as single vacancies.

6. Conclusions

The high-temperature stress anomaly in FeAl with Al content close to 40% is characterised by two important features—that some time is required at the high temperature for strengthening to be obtained [18] and that the observed stress increase is retained when samples are tested at room temperature after quenching. These results strongly suggest that thermally-activated dislocation mechanisms do not play a key role in producing the hardening. Both features support the vacancy-hardening theory [11], whereby the point defects created at high temperature lead to solution hardening, irrespective of whether the material is tested at room or at high temperature. It has not been established before, however, whether these strengthening point defects are present in the form of single vacancies or as multi-vacancy aggregates.

The present study shows no evidence of dislocation pinning by strong obstacles, apart from jogs produced by intersection with forest dislocations. Edge dislocations take up a stepped morphology due to line instabilities for a certain range of directions. Based on a comparison of the experimental strengthening due to high temperature treatments and the likely densities of vacancies or aggregates, it is demonstrated that single vacancies are relatively weak obstacles, leading to only slight dislocation curvature at the obstacle during bypass, while vacancy aggregates such as di- and tri-vacancy aggregates are stronger obstacles that should produce greater dislocation curvature. The lack of experimental evidence of strong dislocation curvature thus supports the idea that the vacancies are probably present as single-vacancy point defects.

Acknowledgements

This research was jointly sponsored by the Division of Materials Science, US Department of Energy, under contract DE-AC05-96OR22464 with Lockheed Martin Energy Rsearch Corporation, and the ORNL SHaRE User facility sponsored by the Division of Materials Science, US Department of Energy under contract DE-AC0576OR00033 with Oak Ridge Associated University. Thanks are due to J.W. Jones, C.A. Carmichael and E.A. Kenik for technical assiatance, and M.H. Yoo, J.M. Schneibel and K. Yoshimi for valuable discussion.

References

[1] Morris DG, Morris MA. Mater Sci and Eng 1997;A239–240:23.
[2] Baker I, Munroe PR. Internat Mater Rev 1997;42:181.
[3] Rosner H, Molenat G, Nembach E. Mater Sci and Eng 1996;A216:169.
[4] Yoshimi K, Hanada S. In: Structural intermetallics. Darolia R, Lewandowski JJ, Liu CT, Martin PT, Miracle DB, Nathal MV. editors. Proc. 1st Int. Conf., TMS, Warrendale, PA, 1993. p 475.
[5] Yoshimi K, Hanada S, Yoo MH. Acta Metall Mater 1995;43:4141.
[6] Morris DG, Morris MA. Intermetallics 1997;5:245.
[7] Morris DG. Phil Mag 1995;A71:1281.
[8] Xiao H, Baker I. Scripta Metall Mater 1993;28:1411.
[9] Baker I, Yang Y. Mater Sci and Eng 1997;A239–240:109.
[10] Kad BK, Horton JA. Mater Sci and Eng 1997;A239–240:118.
[11] George EP, Baker I. Phil Mag 1998;A77:737.
[12] Carleton RL, George EP, Zee RH. Intermetallics 1995;3:433.
[13] Nagpal P, Baker I. Metall Trans 1990;21A:2281.
[14] Chang YA, Pike LM, Liu CT, Bilbrey AR, Stone DS. Intermetallics 1993;1:107.
[15] Rivière JP, Grihle J, Scripta Metall 1975;9:967.
[16] Würschum R, Grupp C, Schaefer HE, Phys Rev Lett 1995;75:97.
[17] George EP, Carleton RL, Zee RH. 1995 (unpublished research, cited in Ref. [18]).
[18] George EP, Baker I. Intermetallics, 1998;6:759.
[19] Schneibel JH, Specht ED, Munroe PR. Mater Sci and Eng 1997;A239–240:245.
[20] Yang Y, Baker I. Intermetallics 1998;6:167.
[21] Yoshimi K, Yoo MH, Hanada S. In: Interstitial and substitutional solute effects in intermetallics. Baker I, Noebe RD, George EP. editors. TMS, Warrendale, 1998, p 39.
[22] Yoshimi K, Yoo MH, private communications.
[23] Fleischer RL. Acta Metall 1963;11:203.
[24] Foreman AJE, Makin MJ. Phil Mag 1966;14:911.
[25] Morris MA, Morris DG. Scripta Mater 1998;38:509.
[26] Crawford RC, Ray ILF, Cockayne DJH. Phil Mag 1973;27:1.
[27] Crawford RC, Ray ILF. Phil Mag 1977;35:549.